Geophys. J. R. astr. Soc. (1987) **89**, 657–679

Explosive volcanic eruptions – VI. Ejecta dispersal in plinian eruptions: the control of eruption conditions and atmospheric properties

L. Wilson* and G. P. L. Walker *Hawaii Institute of Geophysics, 2525 Correa Road, Honolulu, Hawaii 96822, USA*

Accepted 1986 September 29. Received 1986 August 13

Summary. A simple model is developed to relate the maximum down-wind and cross-wind ranges of pyroclasts forming a plinian airfall deposit to the dynamic processes in the eruption cloud from which they fall and the atmospheric wind conditions in the area. The eruption cloud dynamics are in turn related to the eruptive conditions in the vent (vent radius, exsolved magmatic volatile weight fraction, velocity with which material passes through the vent, and mass eruption rate), some or all of which can be deduced if the appropriate field measurements can be made. Some aspects of the stability of convecting volcanic eruption clouds are investigated, and the effects on eruption cloud height of the local atmospheric temperature profile and the value adopted for the entrainment constant (which relates the horizontal flow speed of atmospheric air entering the column to the vertical rise speed of the column material) are explored. It is confirmed that eruption-cloud rise height and pyroclast dispersal are mainly controlled by the mass eruption rate (per unit length of active fissure in the case of linear vents) and, hence, the heat input rate to the cloud; but a significant subsidiary dependence on the amount of exsolved magma volatiles is also found. The eruption cloud model is validated by application to observed historic eruptions, and its use in the analysis of palaeo-eruptions is discussed.

Key words: plinian eruption, ejecta dispersal, atmosphere

Introduction

It has long been recognized that the dispersal of tephra produced in an explosive volcanic eruption is controlled by the height to which clasts are transported in the eruptive column and by the strength of the ambient wind. Thus, intuitively, the dispersal of a pyroclastic fall deposit and, more specifically, the variation of grain size with position in the deposit, will reflect both the size scale of the eruption cloud and the wind speed and direction in the

* Also at Department of Environmental Science, University of Lancaster, Lancaster LA1 4YQ.

atmosphere. Attempts to quantify these relationships for models in which a well-mixed cloud of gas and particles is injected into the atmosphere include those of Knox & Short (1964), Slaughter & Hamil (1970), Shaw, Watkins & Huang (1974), Huang, Watkins & Wilson (1979), Allen (1982) and Suzuki (1983).

To aid the analysis of the dispersal of pyroclasts from such clouds, experimental data were gathered on the terminal fall velocities of pyroclasts in air and analysed in terms of the influence of particle shape on the fall speed by Walker, Wilson & Bowell (1971) and Wilson & Huang (1979). The data were used to derive relationships between dimensionless shape factors and the dimensionless friction-factors and Reynolds numbers, so that terminal velocities can be predicted for any level in any planetary atmosphere; some fall times for pyroclasts released at various heights in the terrestrial atmosphere were given by Wilson (1972).

Later work has been directed at understanding the detailed fluid dynamics of the development of eruption columns. Numerical models were developed by Wilson (1976) and Sparks & Wilson (1976) to describe the interaction with the atmosphere of a plinian eruption column in which a relatively steady and powerful discharge of gas and entrained pyroclasts occurs (Walker & Croasdale 1971). The lower and upper parts of such a column were modelled as a high-speed, inertia-driven gas jet and as a thermally driven convective plume, respectively. It was shown that the maximum height reached by any eruption cloud is determined mainly by the rate at which heat is injected at the base and, hence, by the mass eruption rate through the vent (Wilson *et al.* 1978; Settle 1978). This is in accord with various theoretical models of convecting plumes (Morton, Taylor & Turner 1956; Turner 1979) and experimental data on the heights of industrial plumes summarized by Briggs (1969). Studies of the motions involved in the lowest parts of eruption clouds, where materials are ejected from the vent at generally supersonic velocities, have been made by Kieffer & Sturtevant (1984).

The early dynamic cloud models assumed that the velocity at any height in an eruption cloud was the same at all radial distances from the centre, decreasing abruptly to zero at some well-defined edge of the cloud (a so-called 'top-hat' profile). A more realistic Gaussian profile for the velocity (and other variables) was introduced by Sparks & Wilson (1982) into an improved version of their earlier models, and movie-film measurements of motions within the eruption plume from the 1979 eruption of the Soufriere volcano, St Vincent, were used to constrain the value of the constant which specified the rate of air-entrainment into the cloud.

The most recent theoretical developments in this field have been further enhancements of the Sparks & Wilson (1982) model by Sparks (1986) and Carey & Sparks (1986). In these papers, a method was developed for dealing with the change from largely upward motions in the lower and middle parts of an eruption cloud to largely horizontal motions in the upper part, thus making it possible to predict in more detail than had previously been possible the dispersal of relatively fine-grained material carried into the upper parts of eruption clouds. Carey & Sparks (1986) have inverted this information to deduce eruption cloud heights and wind profiles for specific deposits for which grain size data are available.

In this paper, we explore further the use of the simpler, top-hat velocity profile models. We calculate maximum eruption cloud heights for clouds generated by point-source, conduit-type vents and confirm the fourth-root dependence of eruption cloud height on mass eruption rate of magma from the vent found in several earlier papers. We present the equivalent analysis for a fissure-type, elongate vent and show that, as long as the eruption cloud produced preserves its planar symmetry (which in effect means that it does not rise to a height too much greater than the length of the active fissure), the maximum cloud height is

proportional to the mass flux per unit horizontal length of the fissure raised to the power 1/3, again in accord with theoretical expectations for convecting clouds (Stothers *et al.* 1986).

We show that the simple top-hat models applied to the lower and middle parts of eruption clouds are able to predict the dispersal of a wide enough range of coarse to intermediate size pyroclasts to enable eruption cloud heights (and, hence, mass eruption rates) and wind speeds to be deduced for many deposits. We check our predictions by applying them to measurements on the two deposits for which there are both independent estimates of the eruption cloud height and suitable field data on clast dispersal: the plinian phase of the May, 1980 eruption of Mount St. Helens (Waitt & Dzurisin 1981; Carey & Sigurdsson 1982) and the 1902 eruption of Santa Maria volcano (Williams & Self 1983). We also analyse the deposits of several volcanologically-important prehistoric eruptions examined by Carey & Sparks (1986) so that we can compare our modelling calculations with theirs.

Eruption column dynamics

The major dynamic processes considered to occur in plinian eruption columns have been discussed by Wilson (1976), Wilson *et al.* (1978), Sparks & Wilson (1982) and Sparks (1986). Briefly, a mixture of volcanic gases and pyroclastic particles (in general having a wide range of sizes) is discharged at high velocity through a vent and forms a turbulent jet structure. Rapid mixing of atmospheric air into the column causes rapid deceleration and cooling over a vertical distance equal to about four times the vent diameter. Motions in this initial mixing region are dominated by inertial forces, and this lower zone of the eruption column has been called the 'gas-thrust' region (Sparks & Wilson 1976). In the upper part of the column (the 'convective thrust' region), the buoyancy generated by the heating of entrained air coming into intimate contact with hot pyroclasts becomes the dominant driving force, and the column behaves like a convective plume (Wilson 1976; Wilson *et al.* 1978).

For almost any possible magma volatile content, the bulk density of the mixture of gas and particles emerging from a vent in a plinian eruption (or any relatively steady, magmatic, as distinct from transient or phreatomagmatic, eruption) is greater than the density of the atmosphere. However, this bulk density decreases with height above the vent as pyroclasts are lost from the column and air is entrained into it and heated. At the same time, the upward velocity of the column decreases, partly due to gravity and partly due to the fact that work must be done on the entrained air to sweep it into upward motion. Sparks & Wilson (1976) showed that the proportion of air entrained by a column is controlled by the vent radius, the eruption velocity and the exsolved magma volatile content. They found that some sets of eruption conditions guarantee enough air entrainment to cause buoyancy to win over the decelerating effects, thus allowing a high eruption cloud to form; however, other sets of eruption conditions automatically forbid this, and the erupted material collapses back to the surface forming a fountain over the vent (a 'collapsed' column) feeding pyroclastic flows. Wilson, Sparks & Walker (1980) showed that there was a single-valued relationship between vent radius, released gas content and eruption velocity which allowed any one of these three quantities to be expressed in terms of the other two, thus simplifying the specification of the conditions which lead to convection on the one hand and collapse on the other.

At some level in a convecting eruption cloud, the internal density becomes greater than the surrounding atmospheric density (which is itself decreasing with height as the atmospheric pressure decreases). The cloud material overshoots this level as a result of its inertia and reaches a maximum height from which it settles back as it spreads sideways. When an appreciable horizontal wind field exists in the vicinity of the vent, some material spreads

upwind for a short distance until it reaches a stagnation point, but most of the cloud spreads downwind into a zone lying between the maximum height and the level of neutral buoyancy. The recent work by Sparks (1986) and Carey & Sparks (1986) has greatly improved our understanding of motions in this region.

Support of pyroclastic particles in an eruption column is provided by the net upward motion of the gas. The radius, r_s, of the largest spherical particle of density σ just supported in a gas flow with speed u_v and density ρ is given by

$$(4/3)\pi r_s^3 \sigma g = (0.5)\rho C_D \pi r_s^2 u_v^2, \tag{1}$$

where g is the acceleration due to gravity and C_D is a drag coefficient of order unity if the relative velocity of the clast and the surrounding atmosphere is large enough that the flow regime is turbulent (which will be true for the ranges of clast size and density involved in our analyses). On the basis of a large number of morphological measurements, Blackburn (1977) has shown that the average shapes of Askja pumice clasts (which are typical of pumice clasts in general) are such that equation (1) should be modified to

$$(1.165) r^3 \sigma g = (0.5)\rho C_D (1.608) r^2 u_v^2, \tag{2}$$

where r is the maximum radius (i.e. half the maximum diameter) of an irregular clast and $C_D = 0.8$. Account needs to be taken of the fact that the upward velocity at any point in an eruption cloud is not steady, but consists of a changing, turbulent component superimposed on a mean value. The largest excursion of the velocity from the mean in a very-high Reynolds number system like a plinian cloud will be in the order of 30 per cent (Schlichting 1968) and so the maximum support for a clast will occur when $u_v = 1.3\,u$, roughly, where u is the mean upward gas velocity. Thus equation (2) can be written:

$$\rho u^2 = 0.535\, d\sigma g, \tag{3}$$

where d is the maximum diameter of an irregular clast.

We shall show below that the product ρu^2 almost always decreases monotonically with height in an eruption cloud. Thus, the maximum size of clast that can be supported in the column also decreases with height. We shall also show that the column radius, b (which, in the top-hat velocity profile approximation used here, is defined as the radial distance from the axis of symmetry of the column at which the mean upward velocity changes discontinuously from u to zero), always increases with height in a normal plinian column as mixing with the atmosphere progresses. As a result, the maximum lateral distance from the vent at which a clast with a given size and density will be released increases with decreasing size.

All released clasts will be transported down-wind, and may also experience a translation in a direction perpendicular to the down-wind axis of the fall deposit since the atmospheric wind system is forced to flow around (and, as a result of entrainment, into) the obstacle represented by the eruption column. A distance measured at right angles to the wind direction will be referred to below as a cross-wind distance, and we shall postulate that the cross-wind deflections of clasts released from the cross-wind column edge are minimal. Thus, grain-size variations in the cross-wind direction will be controlled almost entirely by the upward expansion of the eruption column. In particular, the maximum cross-wind range reached by clasts with given values of d and σ is expected to be very closely equal to the radius of the eruption cloud, b, at the height from which they were released. So isopleth maps of maximum grain-size can give directly the variation of $d\sigma$ with b.

Equation (3) can be used to relate values of $d\sigma$ to corresponding values of ρu^2. Our aim, therefore, must be to develop a plinian eruption cloud model in which ρ, u and b can be derived separately as a function of the height, h, above the vent so that $d\sigma$ can be expressed

as a function of b for a given model. The relationship is expected, theoretically, to vary with b_0 and u_0 (the values of column radius and upward gas velocity in the vent) and the released magmatic gas weight fraction, n (Wilson 1976; Wilson *et al.* 1980). The calculations given by Wilson *et al.* (1980) allow any one of these three parameters to be expressed in terms of the other two, or in terms of one of the other two and the mass flux through the vent. Comparison of model-generated graphs of $d\sigma$ as a function of b with 'experimental' data points derived from isopleth maps of specific eruptions will allow some or all of the values of b_0, u_0, n and the mass eruption rate to be obtained.

Eruption column model

The present treatment is an extension of those given by Wilson (1976) and Sparks & Wilson (1982). It retains the simplifying top-hat velocity profile of Wilson (1976) but incorporates the improvements in the treatment of the thermal structure of the eruption column introduced by Sparks & Wilson (1982). The solution of the resulting equations is performed numerically, and without the approximations employed by Sparks (1986) and Carey & Sparks (1986) in solving their model equations.

At any height, h, above the vent let b be the radius of the eruption column (assumed circular in section), u be the mean upward velocity of the gas and all entrained pyroclasts (i.e. those with terminal velocities in the gas much less than u), β be the bulk density of the gas and clasts in the column, θ be the gas temperature, P, θ_a and α be the pressure, temperature and density, respectively, of the surrounding atmosphere; and let the mass flux, M, and the momentum flux, N, be defined by

$$M = \beta u \pi b^2 \tag{4}$$

and

$$N = \beta u^2 \pi b^2. \tag{5}$$

The values of b, u, β, θ, M, N and P in the vent at the base of the cloud are denoted b_0, u_0, β_0, θ_0, M_0, N_0 and P_0, respectively. β_0 is related to n, the exsolved magmatic gas weight fraction in the erupting magma, by

$$(1/\beta_0) = [(nQ\theta_0)/(m_g P_0)] + [(1-n)/\rho_1], \tag{6}$$

where ρ_1 is the density of the non-gaseous part of the magma (which may be a liquid or a mixture of liquid and crystals, depending on the composition and the eruption temperature θ_0, containing accidental fragments of the country rocks forming the walls of the conduit system through which it rises), Q is the universal gas constant (8314 SI units), and m_g is the molecular weight of the volcanic gas species (it is assumed that only one species is present, and for the calculations this is assumed to be H_2O with $m_g = 18$).

All of the atmospheric properties can be expressed as a function of h using a mean atmosphere profile (Valley 1965) for a chosen vent location. The parameters needed to specify any one model eruption are b_0, u_0, θ_0 and n. These are not mutually independent: Wilson *et al.* (1980) have shown that u_0 can be calculated once n, b_0 and θ_0 are chosen, and that the dependence on θ_0 is weak. Furthermore, values of u_0, b_0 and n can be used, via equations (4) and (6), to give corresponding values of M_0, the mass eruption rate. In some parts of our analysis, we shall choose to eliminate u_0 and work in terms of b_0 and n, using an average temperature of $\theta_0 = 1120$ K (appropriate for silicic magmas). Elsewhere, we shall work in terms of the corresponding values of M_0 and n. Table 1 shows the variation of u_0 with b_0 and

Table 1. The variation of eruption velocity in the vent, u_0 (given in $m\,s^{-1}$), with vent radius, b_0, and exsolved magmatic water content, n (in weight per cent), taken from the calculations given by Wilson *et al.* (1980).

b_0	$n = 0.5$	1	2	3	4	5
10	140	200	282	343	399	450
30	145	208	298	370	440	505
100	150	218	315	393	466	530
300	156	225	327	409	483	547
1000	164	230	335	417	490	560

Table 2. Variation of mass flux through the vent, M_0 (in units of $10^6\,kg\,s^{-1}$), with vent radius, b_0 (in m), and exsolved magmatic water content, n (in weight per cent). Values correspond to the velocities given in Table 1.

b_0	$n = 0.5$	1	2	3	4	5
10	1.87	1.35	0.96	0.78	0.68	0.61
30	17.4	12.6	9.08	7.53	6.72	6.17
100	200	147	107	88.9	79.1	72.0
300	1 880	1 370	997	832	737	668
1000	21 900	15 500	11 300	9430	8310	7600

n over the ranges of interest; Table 2 gives the corresponding values of M_0 for the same values of b and n.

The principal equations controlling cloud motion are dictated by the conservation of total mass and momentum. In terms of the variables defined above, these are, respectively (see Sparks & Wilson 1982),

$$(1/M)\,(dM/dh) = (2k/b)\,(\alpha/\beta), \tag{7}$$

where k is the entrainment constant, i.e. the ratio of the horizontal inflow velocity of entrained air at the edge of the column to the vertical velocity, u, and

$$(1/N)\,(dN/dh) = (g/u^2)\,[(\alpha/\beta) - 1]. \tag{8}$$

It is known (Briggs 1969) that the best fit between experimental data and theoretical models of vertical industrial plumes is obtained for a value of k near 0.075 and that, as a plume is blown over into a near-horizontal structure by the wind, the value of k increases to about 0.5. If $k_v = 0.075$ and $k_h = 0.5$ are adopted as the limiting values of k for vertical and horizontal plumes, then a suitable weighted mean of these two values for general use is (Briggs 1969)

$$k = (k_v^2 u^2 + k_h^2 w^2)/(u^2 + w^2), \tag{9}$$

where w is the horizontal wind speed at a given height. The horizontal deflection of the plume is computed by assuming that its horizontal velocity component is the result of the sharing of the accumulated horizontal momentum of the entrained air with the volcanic products, thus being equal to $(n_a w_m)$, where n_a is the fraction of the cloud mass that consists of entrained air and w_m is the mean windspeed between the ground and height h, values being weighted by the entrained air mass over each height increment.

Let the mass fractions of the cloud that consist of volcanic gas and still-entrained

pyroclasts be n_g and n_s, respectively. Mass continuity then requires that

$$n_g = (M_0/M)n \tag{10}$$

and

$$n_s = (M_0/M)K(1-n), \tag{11}$$

where K is the mass fraction of the initial pyroclasts remaining in the column and, by definition, n_a, the mass fraction that consists of entrained air, is

$$n_a = 1 - n_g - n_s. \tag{12}$$

To simulate the progressive release of pyroclasts, K is evaluated at each integration step in any given model calculation by using equation (3) to find the size of the largest pyroclast of any given density that is just retained in the cloud, and then using the data on the variation of cumulative mass with clast size for plinian deposits given by Sparks & Wilson (1976) to find the total mass fraction represented by clasts remaining in the cloud.

The conservation of thermal energy, together with allowance for the effects of adiabatic gas expansion with decreasing total pressure as a given batch of gas in the column rises to greater heights, lead to the relationship

$$\begin{aligned}(c_g n_g + c_a n_a + c_s n_s)\,[(1/\theta)(d\theta/dh) + (1/M)(dM/dh)] &= c_a(\theta_a/\theta)(1/M)(dM/dh)\\ &- c_g(dn_g/dh) - c_a(dn_a/dh) - c_s(dn_s/dh) + (1/P)(dP/dh)\,[\![c_g n_g\,[(\gamma_g - 1)/\gamma_g]\\ &+ c_a n_a\,[(\gamma_a - 1)/\gamma_a]]\!],\end{aligned} \tag{13}$$

where c_a, c_g and c_s are the specific heats of air, volcanic gas and magma, respectively, and γ_g and γ_a are the ratios, for volcanic gas and air, respectively, of the specific heats at constant pressure and constant volume. Finally, the bulk density of the eruption column, β, and the density of the gaseous components alone, ρ, are given by

$$(1/\beta) = [(n_g/m_g) + (n_a/m_a)]\,(Q\theta/P) + (n_s/\rho_1) \tag{14}$$

and

$$(1/\rho) = (Q\theta/P)\,[\![\,[(n_g/m_g) + (n_a/m_a)]/(n_g + n_a)\,]\!]. \tag{15}$$

After considerable algebraic manipulation, including the introduction of the normalized variables b/b_0, u/u_0, β/α, θ/θ_0 and ρ/α to maximize numerical accuracy, the nine equations (7)–(15) can be solved for the nine variables (β, u, b, ρ, θ, k, n_g, n_a and n_s) as a function of h. The solution was programmed in FORTRAN using a simple step-wise numerical integration scheme with automatic adjustment of the vertical height step-length to ensure that fractional changes in the variables never exceeded 1 per cent per step. This constraint was found to yield a good compromise between accuracy and speed; typically, 1300 integration steps were needed per model and the worst accumulated error in any variable was less than 5 per cent.

Preliminary checks and investigations

Model eruption clouds were generated for vent radii, b_0, in the range 10–1000 m and for released magmatic water contents, n, of 0.5–5.0 weight per cent, implying eruption velocities, u_0 in the range 140–560 m s^{-1}; these values in turn imply mass eruption rates, M_0, in the range from 6×10^5 to 2×10^{10} kg s^{-1} (see Table 2), and probably include the values expected for the vast majority of plinian air-fall eruptions (Wilson *et al.* 1978).

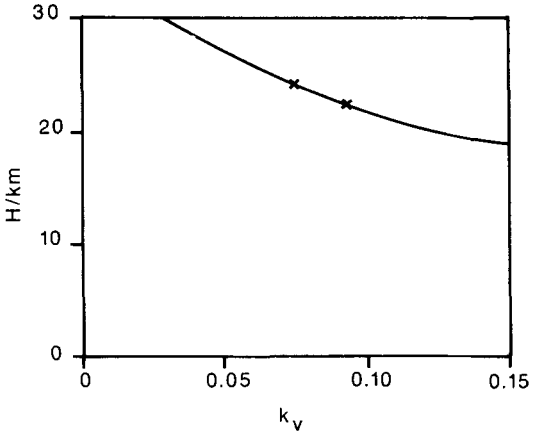

Figure 1. The variation of the predicted eruption cloud height, H, with the value assumed for the air-entrainment constant k_v. The tick marks show the commonly used values of 0.075 and 0.092.

Although the entrainment constant value of $k_v = 0.075$ seems to be appropriate for industrial plumes (Briggs 1969), laboratory experiments have suggested a value close to 0.09 (Rouse, Yih & Humphreys 1952; Morton *et al.* 1956; Turner 1979). The applicability of either of these values to plianian clouds is not yet proven; Sparks & Wilson (1982) discuss this problem and show that the results of their plume modelling calculations are not strongly influenced by the exact choice of value for k_v. We have generated a series of model clouds using values of k_v in the range 0.04–0.15, and the maximum cloud rise height, H, is shown as a function of k_v in Fig. 1. Tick marks on the curve indicate the heights corresponding to $k_v = 0.075$ and 0.09. Even a two-fold error in k_v leads to only a 20 per cent error in the deduced value of H. The value 0.09 is used in subsequent calculations.

A check was made of the extent to which the details of the calculated models depended on the assumed atmospheric properties. Diurnal, seasonal and latitudinal variations in temperature are much larger than corresponding pressure changes, and are known to be dominant in controlling the rise of simple convective plumes (Briggs 1969). Most industrial plumes, like the slowly convecting eruption clouds from intermittently explosive (strombolian or vulcanian) volcanic sources, do not penetrate the tropopause at heights of 10–15 km, whereas, on the basis of observations of historic examples, many plinian eruption columns do. Since variations in atmospheric temperature are generally greater below the tropopause than above, plinian clouds should be less sensitive to temperature variations than industrial plumes. A series of temperature profiles for various seasons and latitudes was taken from Valley (1965) and the rise of a cloud with $b_0 = 70$ m, $n = 0.03$ and hence (Table 1) $u_0 = 390\,\mathrm{m\,s^{-1}}$ was simulated in each profile. The atmospheric temperature at a height of 10 km was chosen as a suitable index of the profile shape, and Fig. 2 shows the variation of maximum cloud height with this index. The vast majority of permutations of season and latitude lead to temperatures at the 10 km level in the range 216–230 K, shown by the tick marks on the plotted curve; the variation of 7 K from the mean value of 223 K leads to a 15 per cent change in H. A standard atmospheric model was chosen for subsequent calculations and its parameters as a function of height are given in Table 3.

Wilson *et al.* (1978) and Settle (1978) showed that data from many observed eruption clouds, and also calculations from earlier, simpler eruption cloud models

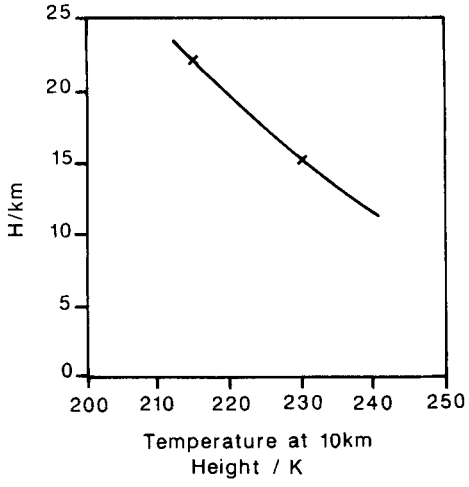

Figure 2. The variation of the predicted eruption cloud height, H, with the value assumed for the atmospheric temperature at a height of 10 km. Almost all temperatures actually encountered in the Earth's atmosphere lie between the tick marks on the curve.

(Wilson 1976), supported the theoretical expectation (Morton *et al.* 1956) that maximum eruption cloud height, H, should be proportional to the fourth root of the heat injection rate into the cloud and, hence, to the fourth root of the mass eruption rate, M_0. The present calculations confirm this relationship for plinian clouds over a wide range of conditions. Fig. 3 shows the variation of H with $M_0^{1/4}$ for various values of n. The relationship begins to break down at large values of M_0 and small values of n for clouds rising to heights greater than 35 km. At heights just greater than this, compressibility effects start to become important in the gas motions (Sparks 1986). As it happens, these circumstances also approach the conditions under which stable convecting eruption clouds cannot in any case form in steady gas-blast eruptions; instead, as noted earlier, the eruption products undergo minimal mixing with the atmosphere and form a low,

Table 3. Values of atmospheric density, α (in kg m^{-3}), and temperature, θ_a (in K), as a function of height, h (in km), adopted as a standard atmosphere profile for model calculations. Data taken from Valley (1965).

h	α	θ_a
0	1.3	280
5	0.77	254
10	0.42	219
15	0.21	217
20	0.089	216
25	0.039	215
30	0.018	217
35	0.0083	227
40	0.0045	240
45	0.0020	260
50	0.0010	265

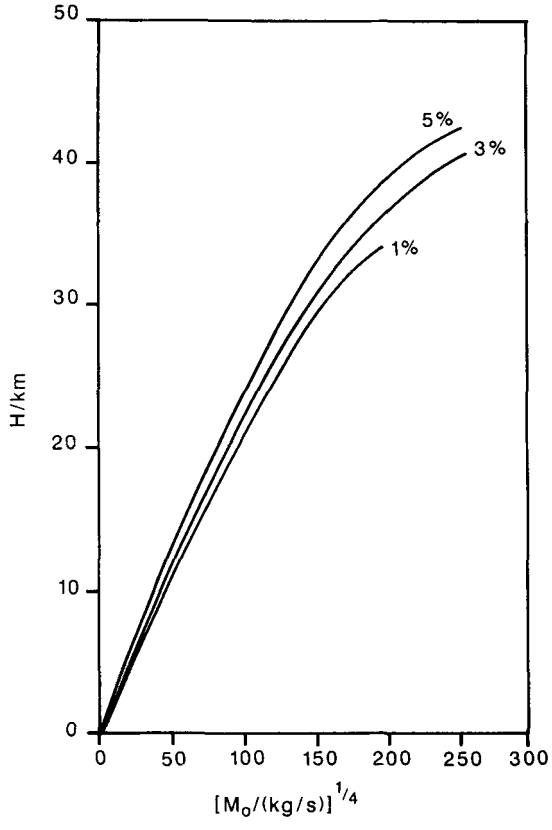

Figure 3. The variation of the predicted eruption cloud height, H, with the mass flux, M_0, from a circular vent for values of n, the exsolved magmatic water weight fraction, of 1, 3 and 5 weight per cent. As indicated by the scale used for M_0, the cloud height is nearly linearly proportional to the fourth root of the mass flux.

'collapsed' fountain over the vent which feeds pyroclastic flows. The function which best fits the mean of the three curves shown in Fig. 3 is

$$H/\text{km} = 0.236\ [M_0/(\text{kg s}^{-1})]^{1/4}, \tag{16}$$

which is the same as the relationship found by Wilson *et al.* (1978) when about 70 per cent of the total heat content of the magma is utilized by the eruption cloud; the efficiency is less than 100 per cent because of the heat carried away by clasts falling out of the cloud.

The ideas outlined so far all apply to eruption from circular vents. Many explosive eruptions may involve elongate, fissure-type vents (e.g. Walker, Self & Wilson 1984), but as long as the eruption cloud from such a vent rises to heights which are much greater than the length of the fissure, the eruption cloud will still have a circular section over most of its height. For cases where the cloud height is comparable to the long axis of the fissure source, equations (4) and (5) require minor modification in that the vent area changes from πb_0^2 to $z_0 L$, where z_0 and L are the short and long axis lengths, respectively, of a rectangular fissure. In the remaining equations, z replaces b, and the numerical constant 2 in equation (7) is replaced with unity. A new relationship is now found between eruption cloud height and magma discharge conditions. The height is con-

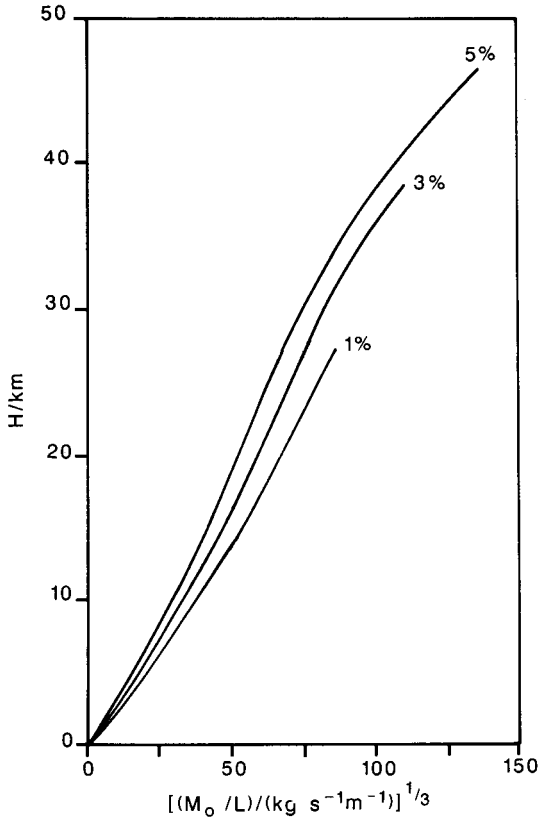

Figure 4. The variation of the predicted eruption cloud height, H, with the mass flux per unit fissure length, M_0/L, from a rectangular fissure vent for values of n, the exsolved magmatic water weight fraction, of 1, 3 and 5 weight per cent. The cloud height is nearly linearly proportional to the mass flux per unit length raised to the power 1/3.

trolled by the mass eruption rate per unit length of fissure, M_0/L, in the manner shown in Fig. 4 for various values of n. The relationship appears to be such that H is proportional to (M_0/L) raised to the power 1/3; Stothers *et al.* (1986) have recently shown that this is the theoretically expected dependence for a line-source of buoyancy.

Model cloud properties

Fig. 5(a)–(f) shows the variation with height of the parameters b, u, θ, β/α, ρ/α and $d\sigma$ for three eruption cloud models. All three models have $n = 0.03$ and are for circular vents with $b_0 = 30$, 100 and 300 m; the curves corresponding to these models are labelled I, II and III, respectively, in all parts of Fig. 5.

All three models show certain common trends. As is to be expected, u (Fig. 5b) and θ (Fig. 5c) decrease with height as entrained air dilutes both the upward momentum and the heat content of the cloud, and b (Fig. 5a) increases, slowly at first and then rapidly as u becomes small. β, the bulk cloud density (Fig. 5d) is greater than the atmospheric density at the vent level (this is true for all values of n less than 12.9 weight per cent for steady eruptions on Earth with water as the magmatic volatile), but air is entrained and heated fast enough in these convectively stable plumes to ensure that β quickly becomes less than α; it

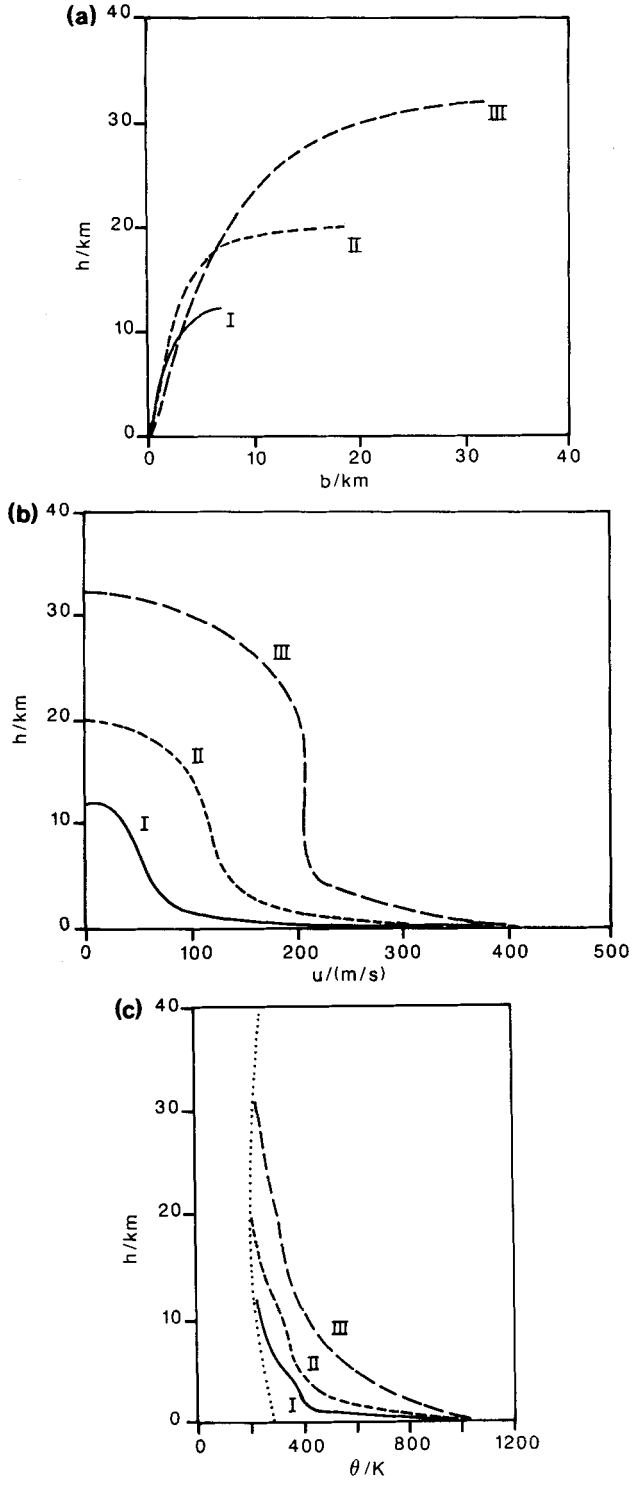

Figure 5. Model parameters generated by calculations for $n = 0.03$ and three values of the circular vent radius b_0. The curves are labelled I, II and III for $b_0 = 30$, 100 and 300 m, respectively. (a) Cloud radius, b, as a function of height, h. (b) Upward gas velocity, u, as a function of height, h. (c) Mean cloud temperature, θ, as a function of height, h; the curve indicated by dots is the model atmospheric profile given in Table 3. (d) The ratio β/α as a function of height, h. (e) The ratio ρ/α as a function of height, h. (f) The product $d\sigma$ as a function of height, h.

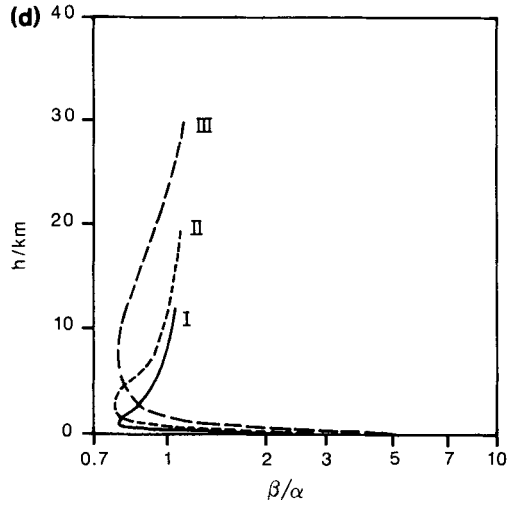

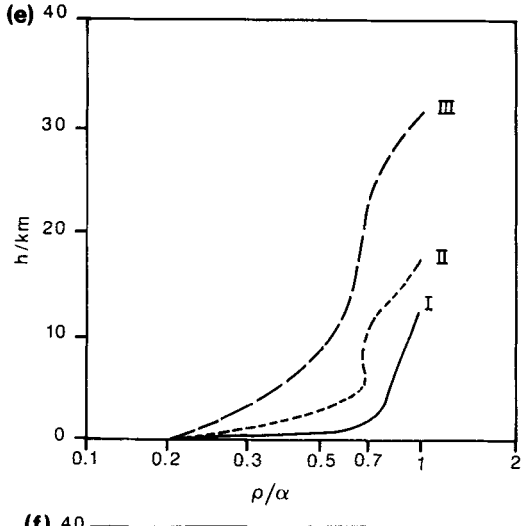

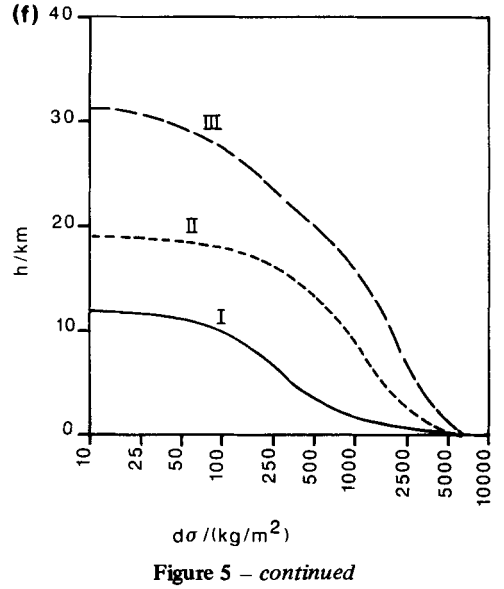

Figure 5 – *continued*

remains so until near the top of the plume where adiabatic cooling eventually causes the cloud to become neutrally buoyant. Its still-appreciable velocity causes the cloud material to overshoot the equilibrium height by about 25 per cent [a figure similar to that found by Sparks (1986) and Carey & Sparks (1986) in their analysis], ultimately settling back to the neutral height as it drifts down wind.

In contrast ρ, the density of the gaseous components of the plume, is much less than the density of the surrounding atmosphere just above the vent level (Fig. 5e), since the only gas present in the column in this region is magmatic steam at high temperature. Addition of cold air causes the overall gas density to increase steadily with height relative to the local air density, and ρ approaches (but is always slightly less than) β. The size, d, calculated from equation (3) for the largest clast of a given density σ which can be supported in the cloud decreases steadily with height (Fig. 5f).

Eruption cloud stability

We have already mentioned the potential instability which threatens convective eruption clouds: if atmospheric air is not mixed sufficiently quickly into the decelerating centre of the plume where the bulk density is greater than the atmospheric density, the cloud material will not convect, but will instead form a relatively low fountain feeding pyroclastic flows. The instability is most easily illustrated by considering the variation of cloud properties with n for a constant value of b_0.

Fig. 6 shows the variation of upward velocity, u (Fig. 6a), and cloud radius b (Fig. 6b), with h for $b_0 = 100$ m and five values of n = 0.675, 0.75, 1, 3 and 5 weight per cent. A small

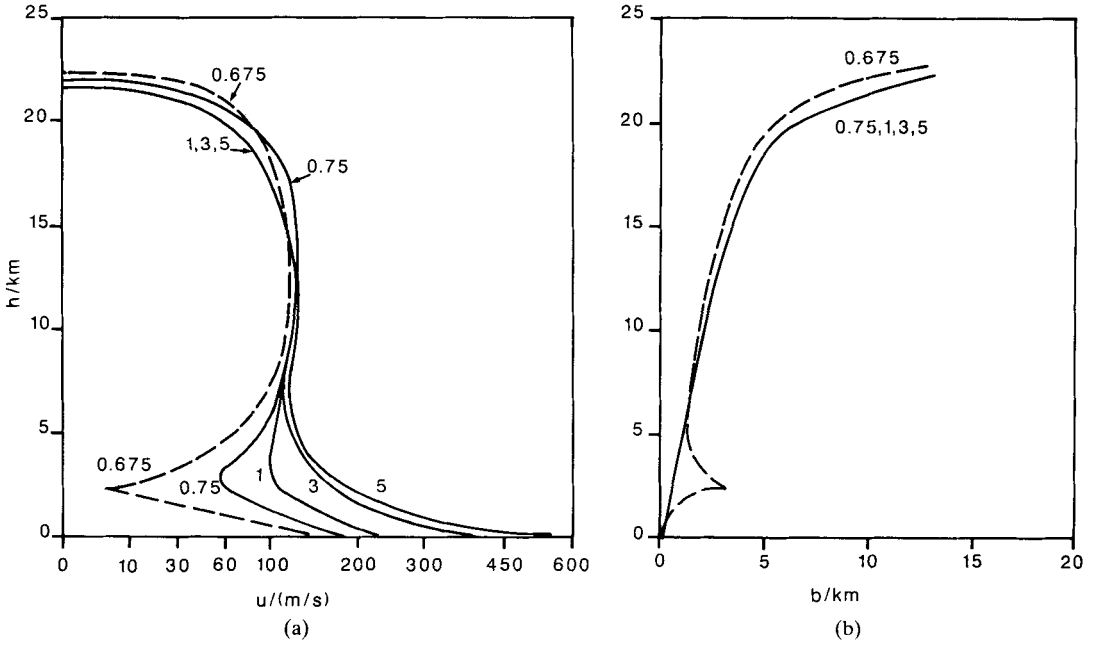

Figure 6. Illustration of the onset of convective instability in an eruption cloud as n is decreased for a constant value of b_0. (a) Variation of upward velocity with height. (b) Variation of cloud radius with height. In each case, the broken line indicates the profile for n = 0.675 weight per cent which is close to the collapse condition; the profiles for n = 0.75, 1, 3 and 5 weight per cent are indistinguishable in (b).

value of n will lead to a relatively low speed for the material leaving the vent, and hence less entrainment of atmospheric air; also, if n is small, the bulk density of the erupted material will be high (6). Both factors act to inhibit convection, and so the onset of instability tends to be abrupt as n is decreased. Fig. 6 confirms these ideas, showing that both the cloud shape and velocity profile are nearly the same for $n = 5$, 3 and 1 weight per cent; however, if n is decreased to 0.675 weight per cent, drastic differences are seen. The upward velocity of the cloud gets very close to zero at a height of 2.2 km, and its width increases rapidly at this level. Collapse to the low fountain configuration is just avoided, and the material accelerates again to high velocities, the cloud shape approaching, but never quite readjusting to, that of the completely stable examples.

It is not clear if a real volcanic cloud should be expected to show the swell and pinch shape shown in Fig. 6b; it is more likely that a cloud this close to instability would show large-scale fluctuations in its properties with time, and would intermittently shed small pyroclastic flows and surges. Such activity cannot be explicitly predicted by our model, however, since it does not deal with the time-dependent aspects of the motion.

A fairly similar pattern of the dependence of instability on n for a constant b_0 is found for other values of b_0 than that shown in Fig. 6. The abruptness of the onset of instability is found to be somewhat less at larger vent radii. The combination of vent radius and exsolved

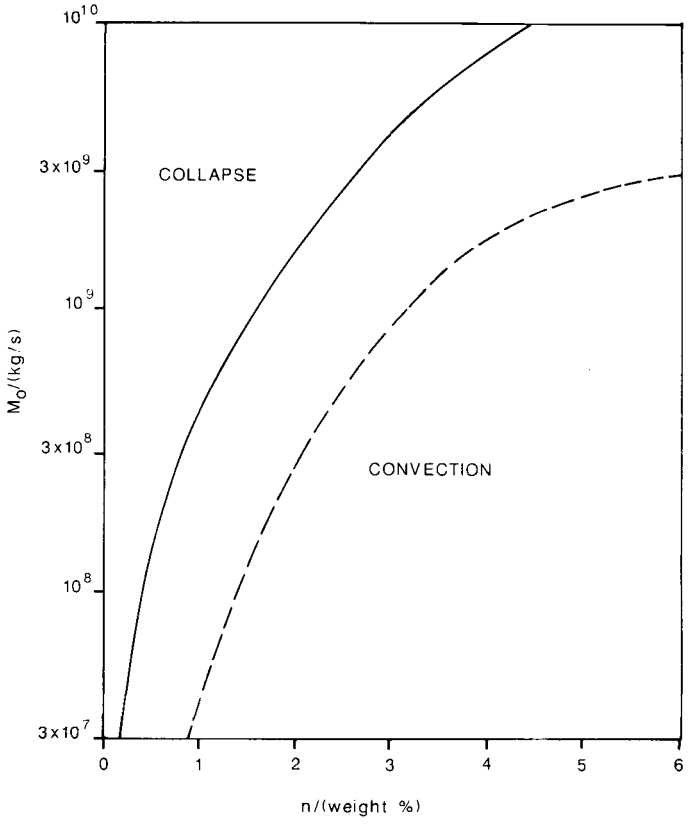

Figure 7. The combinations of mass flux, M_0, and exsolved magma water content, n, which mark the boundary between convectively stable and collapsed eruption columns (solid line). The broken line shows the boundary found by Wilson *et al.* (1980) in earlier eruption cloud models.

gas content (and, hence, implied eruption velocity) at which instability occurs can be used to define the corresponding mass flux. Fig. 7 shows the boundary between the combinations of M_0 and n leading to stable, convecting eruption columns or collapsed columns. Also shown is the position of the boundary as given by Wilson *et al.* (1980); their calculations were based on the earlier generation of eruption cloud models reported by Wilson (1976) and Sparks & Wilson (1976). The present calculations suggest that the boundary lies at a lower gas content (by at least one weight per cent) for a given mass flux than the values found earlier. This finding does not change the qualitative sense of any of the conclusions presented in the above and other papers about the consequences of column instability; it does, however, underline the fact that the stability criterion is very sensitive to the model assumptions, and that much more work is needed to understand the exact details of the processes occurring at the base of an eruption cloud.

Pyroclast dispersal

The calculations equivalent to those shown in Fig. 5 have been performed for a wide range of possible eruption conditions. The first step in the use of this information is the combina-

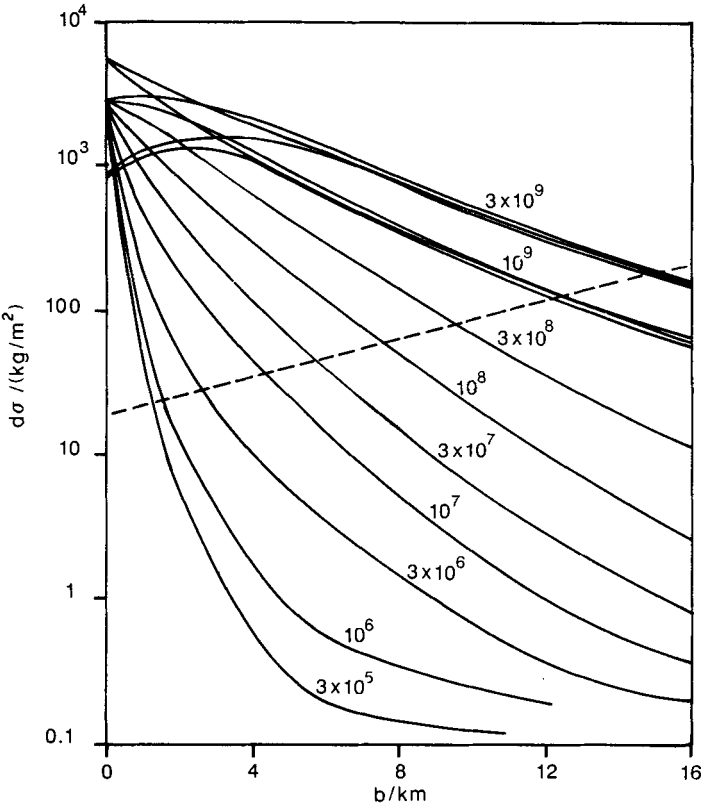

Figure 8. Values of clast size multiplied by density, $d\sigma$, plotted as a function of b, the eruption cloud radius at the height from which they were released (now identified as being equal to the maximum cross-wind range which clasts with these properties can reach) and M_0, the mass flux erupted from the vent. For $M_0 = 10^9$ and 3×10^9 kg s^{-1}, the curves are shown separately for $n = 1$ (lower curve), 3 (middle curve) and 5 (upper curve) weight per cent; for the other mass fluxes, only the curve for $n = 3$ weight per cent is shown. These predictions are expected to be reliable only in the region above the broken line, which corresponds to clasts released from the lower half of the corresponding eruption cloud, for the reasons discussed in the text.

tion of the equivalents of Figs 5(a) and (f) to give the product $d\sigma$ as a function of b. It will be recalled that clasts released from the edge of an eruption column, at a distance b from the axis of symmetry, are postulated to drift downwind with little deflection at right angles to the downwind direction, and to reach the ground at a distance b from the downwind axis of the fall deposit; thus the graph of $d\sigma$ as a function of b should represent the maximum cross-wind ranges of clasts having a given size and density. The information can be plotted in many ways, since the relationship between $d\sigma$ and b is expected to be a function of some or all of u_0, b_0, n and M_0.

It is found that, except in the immediate vicinity of the vent, $d\sigma$ plotted as a function of b depends strongly on M_0 and also has a subsidiary dependence on n (thus resembling, in many respects, the behaviour of H). The relationship is shown in Fig. 8 for several values of M_0 and three values of $n = 1$, 3 and 5 weight percent exsolved magmatic water. It can be seen that, very close to the vent, $d\sigma$ loses its dependence on M_0 and becomes almost entirely a function of n. This is because, as shown by equation (3), the supporting drag force acting on pyroclasts emerging from the vent depends on the gas density, ρ, and the gas velocity, u; ρ depends on the magma temperature and the local atmospheric pressure (assuming that the gas is, in fact, able to decompress to atmospheric pressure at the vent – see Wilson *et al.* 1980) and u is essentially proportional to the square root of n (see Wilson 1980). Above the vent, both ρ and u soon become dominated by the consequences of air entrainment. Wilson (1976) suggested that gas velocities (and, hence, released magmatic volatile weight fractions) could be determined by measuring the sizes of the largest clasts of a given density which were just able to be erupted, and that these limiting sizes might be extrapolated from near-vent size data. Fig. 8 shows that such data must be collected from within about 2 km of the vent in order to be used for such a purpose.

It will be recalled that our model is not expected to be reliable for predicting the dispersal of small clasts released from the upper parts of eruption clouds, since it is in these regions that the excessive lateral spreading of the cloud investigated by Sparks (1986) and Carey & Sparks (1986) becomes important. To emphasize this expectation we have marked with a broken line in Fig. 8 the boundary between pyroclasts falling from the upper and lower halves of the model eruption clouds.

Analyses of eruption deposits

MASS FLUXES AND ERUPTION CLOUD HEIGHTS

We have tested the clast dispersal predictions implied by Fig. 8 using field measurements of grain size variations for the same set of two historic eruptions and five prehistoric (but volcanologically important) eruptions used by Carey & Sparks (1986). Fig. 9a shows cross-wind dispersal data from the plinian phase of the 1980 May eruption of Mount St Helens (Waitt & Dzurisin 1981; Carey & Sigurdsson 1982), the 1902 eruption of Santa Maria (Williams & Self 1983), and the 1875 eruption of Askja (Sparks, Wilson & Sigurdsson 1981). Fig. 9b shows data for the 1886 eruption of Tarawera, New Zealand (Walker *et al.* 1984), the Fogo A and Fogo 1563 deposits (Walker & Croasdale 1971), and the Taupo ultra-plinian deposit (Walker 1980).

The expectation that our model will not deal adequately with the dispersal of small pyroclasts released from the upper half of an eruption cloud is clearly fulfilled by the data in Fig. 9 – at decreasing values of $d\sigma$ the plotted data points lie at systematically greater cross-wind ranges than is consistent with any one of our constant-mass-flux curves. We take as our best estimate of the mass flux for a given deposit that value for which the corresponding

curve calculated for $n = 3$ weight per cent in Fig. 9 would lie among the proximal data points. Using this criterion, we obtain the mass fluxes shown in Table 4. Also shown are the cloud heights deduced from these mass fluxes using equation (16), the observed cloud heights for the two cases where information is available, and the cloud heights deduced by Carey & Sparks (1986) in their analysis.

There is quite good agreement between the mass fluxes found by ourselves and by Carey & Sparks (1986); there are, however, systematic differences between the implied cloud heights. It is not surprising that there should be some differences, of course, since both treatments make numerous approximations, the most critical of ours being the assumption of the top-hat velocity profile. We expect that our mass flux values should be relatively reliable

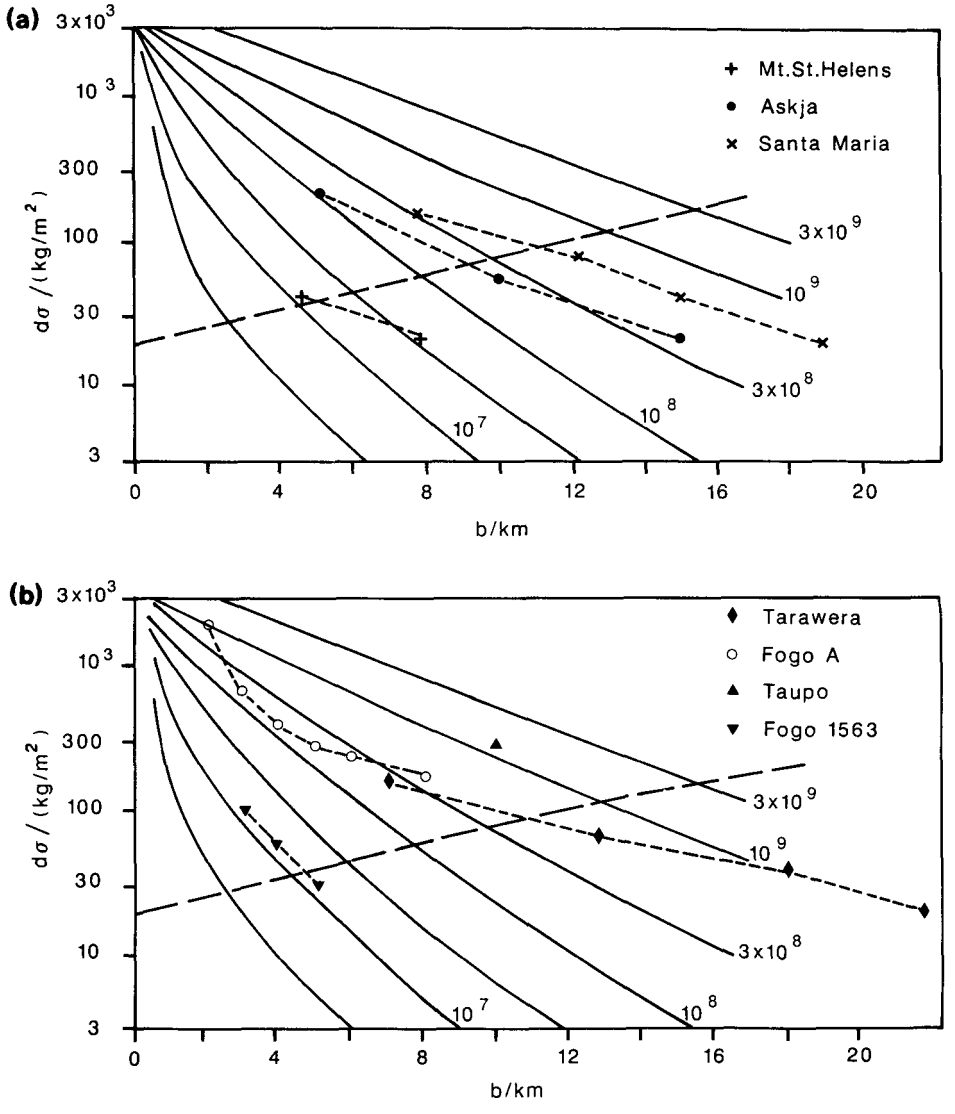

Figure 9. Cross-wind clast dispersal data. Maximum cross-wind clast ranges are shown for several values of $d\sigma$ for each eruption analysed the definitions and labelling of the axes and curves are the same as in Fig. 8.

Table 4. Maximum eruption cloud height estimates, H (in km), and mass eruption rates, M_0 (in kg s^{-1}), for various eruptions.

Eruption	H from direct observation	M_0 (this analysis)	H	M_0 (Carey & Sparks 1986)	H
Mt St Helens	19	2.3×10^7	16	2.2×10^7	19
Santa Maria	28 and 48	3.2×10^8	32	2.2×10^8	34
Fogo 1563	–	1.2×10^7	16	1.9×10^7	18.5
Askja	–	9.0×10^7	23	7.7×10^7	26
Fogo A	–	1.7×10^8	27	1.4×10^8	30
Tarawera	–	2.3×10^8	29	2.2×10^8	34
Taupo	–	2.0×10^9	50	1.1×10^9	51

(within the limitations of the model assumptions) since they are dictated by the match between field observations and calculated cross-wind clast ranges derived from the lower part of the eruption column, where the complications caused by the lateral expansion of the cloud (as modelled by Carey & Sparks) are a minimum. The agreement between the mass flux values is most satisfactory, since the major aim of developing these kinds of analyses is the reconstruction of eruption conditions in prehistoric eruptions, and the mass flux is a volcanologically more significant quantity than the cloud height.

The differences in cloud height estimates stem mainly from the fact that Carey & Sparks appear to relate mass flux to cloud height using a larger value for the fraction of particles retained in an eruption cloud at a given height, and hence for the efficiency of heat utilization, than implied by our calculations: although they do not say exactly how they carry out the conversion, it is clear from their pairs of values of mass flux and cloud height that, for a given magma temperature, the numerical constant in their equivalent of our equation (16) is larger than our value by a factor of about 1.19. Our cloud heights are likely to be somewhat too small, since our models do not have as much lateral expansion in their upper parts as those of Carey & Sparks, and thus entrain rather too much air which dilutes the upward momentum; the cloud heights of Carey & Sparks may be somewhat too large, since their treatment does not take detailed account of the progressive heat loss from the cloud which occurs as clasts are released from it.

WIND-SPEED ESTIMATES

In order to obtain estimates of the wind speed relevant to each of the eruptions analysed we have used a similar procedure to that of Carey & Sparks (1986). Whenever the value of $d\sigma$ for clasts released from the edge of a model cloud changes by a factor of two we record the release height and follow the path of the clast numerically as it settles through an appropriate wind profile. Carey & Sparks employed the same standard wind-speed profile for all of the eruptions they analysed. We have taken instead the annual average wind-speed profile for the geographical region in which the volcano is located from data in Valley (1965).

Given the expected limitations of our model, we have elected not to make any allowance for the disturbance of the wind field by the presence of the eruption column; we anticipate that, as far as the maximum down-wind transport of clasts is concerned, any local increases in wind speed near the column edge dictated by mass continuity requirements will be approximately compensated by the radial inflow of air into the column.

Fig. 10 shows the annual average wind-speed profiles used for the eruptions analysed; Table 5 gives, for each eruption, the factor by which the local wind profile must be multi-

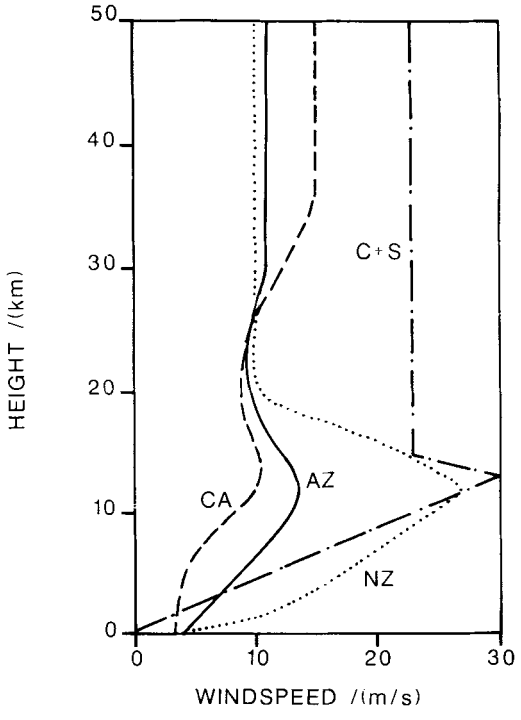

Figure 10. Examples of annual average vertical wind-speed profiles for some of the geographical locations of the eruptions shown in Tables 4 and 5. Data from Valley (1965). NZ: North Island, New Zealand; AZ: Azores; CA: Central America. C+S is the wind profile used by Carey & Sparks (1986).

plied to give the best fit to the down-wind transport of clasts. These factors were found by taking the down-wind ranges of several grain-sizes from isopleth maps, subtracting from each down-wind range the corresponding cross-wind range computed for the same grain-size and clast density, and then dividing each difference by the computed range using the standard wind profile; the wind profile factor is then taken to be the arithmetic mean of these ratios. Also shown in Table 5 are the implied values of the wind speed at the tropopause, and the corresponding value deduced by Carey & Sparks (1986).

Table 5. Values of the factor by which the annual average wind-speed profile must be multiplied to yield agreement with the observed down-wind transport of pyroclasts for several eruptions. Also given are the implied wind speed at the height of the tropopause, the value of the tropopause-level wind found by Carey & Sparks (1986), and the observed speed in the two cases where estimates are available. All wind speeds are in $m\,s^{-1}$.

Eruption	Wind factor (this work)	Tropopause wind (this work)	Tropopause wind (Carey & Sparks)	Observed wind speed
Mt St Helens	1.9	27	36	30
Santa Maria	1.4	15	14	–
Fogo 1563	2.1	29	25	–
Askja	1.4	19	28	25
Fogo A	0.35	5	0	–
Tarawera	0.3	8	4	–
Taupo	1.9	50	27	–

For some of the eruptions, the agreement between the two analyses is satisfactory. However, our analysis gives a substantially lower wind speed than that of Carey & Sparks for the Askja event, a substantially higher value for each of the Tarawera and Taupo eruptions, and a non-negligible wind speed for the Fogo A deposit. These differences can by no means be explained as the consequence of our using different wind profiles, since the relative shapes of the various profiles that we and they have employed (Fig. 10) are inevitably quite similar, and seem to be a fundamental consequence of the differences between our dynamic cloud models. As was the case for eruption cloud heights, there are very few independent wind-speed estimates to use as checks on these calculations; those that are available are shown in Table 5, and we note that our estimates and those of Carey & Sparks (1986) appear to bracket the observed speeds.

One reason for carrying out the wind-speed analysis in terms of factors by which the annual average wind must be multiplied is that this affords us another way of carrying out a check on the accuracy of our model. Any one eruption may occur under conditions ranging from calm through typical to stormy conditions, and at any time of year. However, there appears to be no reason to expect a correlation between weather conditions or time of year and the onset of explosive eruptions. Hence, if the wind profile multiplication factor can be determined for a large enough number of eruptions, the mean value is expected to approach unity. We have carried out the equivalent analyses to those described here for 26 additional eruptions (the details of which will be described elsewhere) and find that there is a total of 10 additional instances in which acceptable estimates of wind speed can be made. The mean wind-speed factor found for these 17 cases is 1.3 ± 0.6; this value is not significantly different from unity, and we take this to indicate that there is no evidence for gross systematic errors in the predictions of our model, despite its many approximations.

Conclusions

We have described a model for the dynamic conditions in a plinian eruption cloud which appears to be adequate to relate the dispersal of pyroclasts to the eruption conditions in the vent. The model has allowed us to confirm the relationship between cloud height and mass flux from the vent (16) deduced from earlier, simpler models and also found in the more detailed model developed by Carey & Sparks (1986).

In addition, we have been able to define the equivalent relationship (17) for line-source (fissure-vent) type eruptions. We have explored in more detail than has been possible before the dependence of eruption cloud height and pyroclast dispersal on the values adopted for the entrainment constant which determines the rate of ingestion of atmospheric air into an eruption cloud (Fig. 1), on the temperature profile of the local atmosphere (Fig. 2), and on the separate values of total mass flux and released magma gas content (Figs 3, 4 and 8). This has enabled us to define the ranges of mass flux and magma gas content within which convective eruption clouds are stable in the Earth's atmosphere (Fig. 7).

Despite some systematic differences in cloud height estimates, our model produces eruption mass flux values and ambient wind-speed estimates which are generally similar to those of Carey & Sparks (1986) and which are consistent with the (meagre) independent estimates for historic eruptions.

Acknowledgments

L.W. received partial support for this work via Research Grants from the Leverhulme Foundation (UK) and the Royal Society; the Department of Geology of the University of

Auckland generously provided computer facilities for some of the calculations. G.P.L.W. carried out fieldwork on the New Zealand pumice deposits while Captain James Cook Research Fellow of the Royal Society of New Zealand. We thank Steve Sparks, Steve Carey and Gillian Thornhill for constructive discussions about the formulation of the modelling equations, and Jane Rushton for preparing the diagrams. H.I.G. Contribution Number 1829.

References

Allen, J. R. L., 1982. *Sedimentary Structures, their Character and Physical Basis,* Elsevier, Amsterdam.

Blackburn, E. A., 1977. Some aspects of explosive volcanism on the Earth, Moon and Mars, *PhD thesis,* University of Lancaster, UK.

Briggs, G. A., 1969. Plume rise. *Critical Review Series, Report TID-25075,* pp. 1–81, Atomic Energy Commission, Washington, DC.

Carey, S. & Sigurdsson, H., 1985. The May 18, 1980, eruption of Mount St. Helens 2, Modelling of the dynamics of the plinian phase, *J. geophys. Res.,* **90,** 2948–2958.

Carey, S. & Sparks, R. S. J., 1987. Quantitative models of the fall-out and dispersal of tephra from volcanic eruption columns, *Bull. volcan* (in press).

Huang, T. C., Watkins, N. D. & Wilson, L., 1979. Deep-sea tephra from the Azores during the past 300,000 years: eruptive cloud height and ash volume estimates, Part I: *Bull. geol. Soc. Am.,* **90,** 131–133; Part II: *Bull. geol. Soc. Am.,* **90,** 235–288.

Kieffer, S. & Sturtevant, J. B., 1984. Laboratory studies of volcanic jets, *J. geophys. Res.,* **89,** 8253–8268.

Knox, J. B. & Short, N. M., 1964. A diagnostic model using ash-fall data to determine eruption characteristics and atmospheric conditions during a major volcanic event, *Bull. volcan.,* **27,** 5–24.

Morton, B. R., Taylor, G. & Turner, J. S., 1956. Turbulent gravitational convection from maintained and instantaneous sources, *Proc. R. Soc. A,* **234,** 1–23.

Rouse, H., Yih, C. S. & Humphreys, H. W., 1952. Gravitational convection from a boundary source, *Tellus,* **4,** 201–210.

Schlichting, H., 1968. *Boundary Layer Theory,* McGraw-Hill, New York.

Settle, M., 1978. Volcanic eruption clouds and the thermal power output of explosive eruptions, *J. Volcanol. Geotherm. Res.,* **3,** 309–324.

Shaw, D. M., Watkins, N. D. & Huang, T. C., 1974. Atmospherically transported volcanic glass in deep-sea sediments: theoretical considerations, *J. geophys. Res.,* **79,** 3087–3094.

Slaughter, M. & Hamil, M., 1970. Models for deposition of volcanic ash and resulting bentonite. *Bull. geol. Soc. Am.,* **81,** 961–968.

Sparks, R. S. J., 1986. The dimensions and dynamics of volcanic eruption columns, *Bull. volcan.,* **48,** 3–15.

Sparks, R. S. J. & Wilson, L., 1976. A model for the formation of ignimbrite by gravitational column collapse, *J. geol. Soc. Lond.,* **132,** 429–440.

Sparks, R. S. J. & Wilson, L., 1982. Explosive volcanic eruptions–V. Observations of plume dynamics during the 1979 Soufriere eruption, St. Vincent, *Geophys. J. R. astr. Soc.,* **69,** 551–570.

Sparks, R. S. J., Wilson, L. & Sigurdsson, H., 1981. The pyroclastic deposits of the 1875 eruption of Askja, Iceland, *Phil. Trans. R. Soc., A,* **299,** No. 1447, 242–273.

Stothers, R. B., Wolff, J. A., Self, S. & Rampino, M. R., 1986. Basaltic fissure eruptions, plume heights and atmospheric aerosols, *Geophys. Res. Lett.* (submitted).

Suzuki, T., 1983. A theoretical model for the dispersal of tephra, in *Arc Volcanism: Physics and Tectonics,* pp. 95–113, eds Shimozuru, D. & Yokoyama, I., Reidel, Dortrecht.

Turner, J. S., 1979. *Buoyancy Effects in Fluids,* Cambridge University Press.

Valley, S. L., 1965. in *Handbook of Geophysics and Space Environments,* Chapter 4, McGraw-Hill, New York.

Waitt, R. B. & Dzurisin, D., 1981. Proximal air-fall deposits from the May 18 eruption–stratigraphy and field sedimentology, *U.S.G.S. Prof. Paper 1250,* 601–616.

Walker, G. P. L., 1980. The Taupo pumice: product of the most powerful known (ultraplinian) eruption? *J. Volcanol. Geotherm. Res.,* **8,** 69–94.

Walker, G. P. L. & Croasdale, R., 1971. Two plinian-type eruptions in the Azores, *J. geol. Soc. Lond.,* **127,** 17–55.

Walker, G. P. L., Wilson, L. & Bowell, E. L. G., 1971. Explosive volcanic eruptions–I. The rate of fall of pyroclasts, *Geophys. J. R. astr. Soc.,* **22,** 377–383.

Walker, G. P. L., Self, S. & Wilson, L., 1984. Tarawera 1886 New Zealand – a basaltic plinian fissure eruption, *J. Volcanol. Geotherm. Res.*, **21**, 61–78.

Williams, S. N. & Self, S., 1983. The October 1902 plinian eruption of Santa Maria volcano, Guatemala, *J. Volcanol. Geotherm. Res.*, **16**, 33–56.

Wilson, L., 1972. Explosive volcanic eruptions–II. The atmospheric trajectories of pyroclasts, *Geophys. J. R. astr. Soc.*, **30**, 381–392.

Wilson, L., 1976. Explosive volcanic eruptions–III. Plinian eruption columns, *Geophys. J. R. astr. Soc.*, **45**, 543–556.

Wilson, L., 1980. Relationships between pressure, volatile content and ejecta velocity in three types of volcanic explosion, *J. Volcanol. Geotherm. Res.*, **8**, 297–313.

Wilson, L. & Huang, T. C., 1979. The influence of shape on the settling velocity of volcanic ash particles, *Earth planet. Sci. Lett.*, **44**, 311–324.

Wilson, L., Sparks, R. S. J. & Walker, G. P. L., 1980. Explosive volcanic eruptions–IV. The control of magma chamber and conduit geometry on eruption column behaviour, *Geophys. J. R. astr. Soc.*, **63**, 117–148.

Wilson, L., Sparks, R. S. J., Huang, T. C. & Watkins, N. D., 1978. The control of volcanic column height by eruption energetics and dynamics, *J. geophys. Res.*, **83**, 1829–1836.